Soft Matter

The Tripeptide GHG as an Unexpected Hydrogelator Triggered by Imidazole Deprotonation

Journal:	*Soft Matter*
Manuscript ID	SM-COM-02-2020-000224.R1
Article Type:	Communication
Date Submitted by the Author:	29-Jan-2020
Complete List of Authors:	Hesser, Morgan; Drexel University, Department of Chemistry Thursch, Lavenia; Drexel University, Department of Chemical and Biological Engineering Lewis, Todd; Drexel University, Department of Chemical and Biological Engineering DiGuiseppi, David; Drexel University, Deparment of Chemistry; Drexel University Alvarez, Nicolas; Drexel University, Schweitzer-Stenner, Reinhard; Drexel University, Chemistry

COMMUNICATION

The Tripeptide GHG as an Unexpected Hydrogelator Triggered by Imidazole Deprotonation

Received 00th January 20xx,
Accepted 00th January 20xx

DOI: 10.1039/x0xx00000x

Morgan Hesser,[a] Lavenia Thursch,[b] Todd Lewis,[b] David DiGuiseppi,[a] Nicolas Alvarez[b] and Reinhard Schweitzer-Stenner [a]

The tripeptide glycyl-histidyl-glycine (GHG) self-assembles into long, crystalline fibrils forming a strong hydrogel (G'~50 kPa) above a critical concentration of 40 mM upon the deprotonation of its imidazole group. Spectroscopic data reveal a mixture of helically twisted β-sheets and monomers to coexist in the gel phase.

Over the last 10 years short peptides (di- and tri- peptides) have emerged as cost-effective building blocks for supramolecular ensembles such as nanotubes and gels.[1–6] It is generally believed that the self-assembly of peptides into fibrils requires amino acid residues with aromatic side chains and end groups (e.g. Fmoc: Fluorenylmethyloxycarbonyl). Fmoc has been shown to engage in hydrophobic interactions and cation-π interactions, both of which contribute to self-assembly.[4,7,8,9] However, this notion has been challenged recently by the discovery that the unblocked cationic tripeptide with the sequence GAG self-assembles into large scale fibrils, which at high concentrations form a sample spanning network.[10–12] In line with the earlier emphasized role of side chain aromaticity, DiGuiseppi et al. discovered that upon deprotonation of its imidazole group, GHG forms similarly large scale fibrils in water.[13] If the network formed by GHG deprotonation is a gel, it will be more suitable for biomedical applications than other low molecular weight peptides since its formation does neither involve organic solvents nor very acidic or alkaline conditions.[14] Deprotonated imidazole groups have been shown before to provide gelator capability to peptide derivatives, but such compounds either contained additional aromatic moieties and aliphatic chains[15,16] or multiple imidazole groups.[17,18] Using Fmoc as a capping group has been shown to increase aggregation of the histidine containing dipeptide L-carnosine,[19] even at pH 3 where the imidazole group of the histidine residue is actually protonated. In this communication, we show that under the right conditions, namely pH values favoring the deprotonated state of the imidazole, the unblocked tripeptide GHG (Figure S1) self-assembles into long fibrils in "haystack"-like aggregates with remarkable rheological properties despite lacking additional groups that favor gelation.

Our initial step was to create a phase diagram which illustrates how the critical concentration for the fibrilization of GHG depends on pH. To this end, we first dissolved the peptide in water at acidic pH (between 2 and 3) in Eppendorf cuvettes and subsequently titrated the sample to the desired pH by adding an appropriate amount of NaOH (cf. Material and Methods). An image of the samples produced at various pH and peptide concentrations is shown in Figure S2. Thus, we obtained the phase diagram in Figure 1, wherein filled circles denote experimental conditions probed. No visible fibril aggregates were obtained in the red region of the phase diagram after 2 weeks. The yellow area denotes a region where large fibrils became visible while the sample was inhomogeneous and transparent. In the green region, conditions allow for a significant number of aggregates to form such that the samples were opaque (Figure S2). Overall, the phase diagram in Figure 1 reveals a critical concentration of ca. 40 mM below which we did not observe large size aggregation irrespective of the pH value. When samples in the green region were subjected to the addition of acid, the sol state of the system was recovered. Hence, the obtained phase transition is reversible.

The pK-value of the imidazole group of histidine in water is 6. This value can move up or down in peptides and proteins, depending on the respective environment.[20] The phase diagram in Figure 1 suggest that self-assembly initiates just below the pK-value of the imidazole group. In order to provide a suitable reference point, we measured the UV-circular dichroism (UVCD) spectra of GHG as a function of pH between 2 and 11 for a peptide concentration of 10 mM, which lies below the critical concentration for large scale self-assembly. As shown in Figure S3, the UVCD spectrum is clearly pH-dependent which reflects the different degree of electronic coupling between imidazole and peptide backbone transitions in the two protonation states.[21,22] The measured spectra depict an isodichroic point within the limits of spectral noise, which indicates the expected two-state transition. Figure S2 displays the dichroism value measured at 195 nm, $\Delta\varepsilon_{195}$, as a function of pH. A Henderson-

[a] *Department of Chemistry*
Drexel University
3141 Chestnut Street, Philadelphia, PA 19104, USA
E-mail: rschweitzer-stenner@drexel.edu.
[b] *Department of Chemical and Biological Engineering,*
Drexel University,
3141 Chestnut Street, Philadelphia, PA 19104Address here.
Electronic Supplementary Information (ESI) available: See DOI: 10.1039/x0xx00000x

Hasselbach type analysis yielded a pK-value of 6.48±0.08. The phase diagram in Figure 1 indicates that the critical pH for concentration decreases from ca. 6.4 to 5.8 upon increasing the peptide concentration from 40 to 300 mM. From this result it follows that the self-assembly of GHG leads to a substantial downshift of the critical pH by up to 0.6 units. This observation reflects the fact that a critical number of fibrils for large scale aggregation becomes available at lower pH.

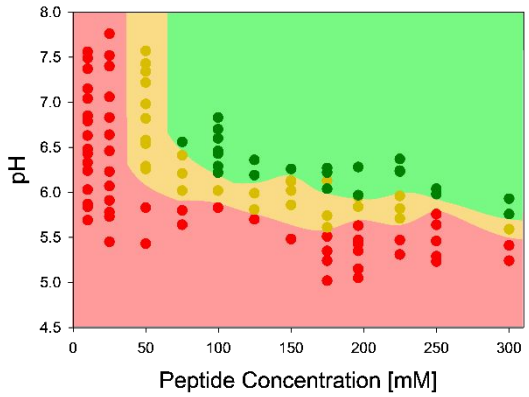

Figure 1. Phase diagram of GHG in water with respect to peptide concentration and solution pH. Samples were characterized visually as those showing no visible large-scale peptide aggregates (red dots), those with partial aggregation (yellow dots), and nearly complete aggregation (green dots). The background has been added as a visual guide for the identification of phases.

Microscopy, rheology, and spectroscopy were all performed on a sample with 175 mM GHG within a pH close to 6.4 which lies in the green area just above the boundary between the yellow and green areas as well close to center of the range of concentrations used for the well plate experiment. Figure 2 shows a microscope image of a GHG sample at pH=6.4 (cf. Material and Methods). The sample spanning network can be described as overlapping various sized "haystacks" composed of comparatively needle-like fibrils with lengths in the sub-millimeter regime. The haystacks appear intertwined or entangled, which is expected to lead to a volume spanning network, i.e. hydrogel. At these conditions, the fibril network is relatively sparse, and the pore size is very large. We expect that the pore size is a strong function of GHG concentration. Note that these structures are very different than the "sea urchin"-like structures formed by GAG in water-ethanol mixtures.[12] They are qualitatively different from the much shorter and thinner nano-scale fibrils formed by aromatically blocked FmocFF and its derivatives.[2,6,8]

Rheological tests were conducted to determine whether a volume spanning network was formed by the haystack aggregates. The result of a frequency sweep spanning four orders of magnitude (10^{-2} to 100 rad s^{-1}) of 175 mM GHG at pH=6.4 is shown in Figure 3. The amplitude strain used was 0.03%. At this value we are somewhat outside the linear viscoelastic regime for the highest frequencies (see amplitude sweep in Figure S5) but this allows us to apply a deformation that is within machine limits. The storage modulus is higher than the loss modulus (respectively 44 kPa and 11 kPa for ω= 1 rad s^{-1}) which is indicative of a viscoelastic gel. The G' value is relatively high which is to be expected of the long, entangled fibrils observed in Figure 2. However, G' is lower than values previously reported for GAG water/ethanol gels, which may be due to the large pores observed throughout the network. At low frequency, the moduli get closer to each other and tan δ increases from 0.28 to 0.68, reflecting a more viscous response. We also obtained the softening point of 175 mM GHG at pH=6.4 to be 58 °C using a method previously employed for GAG in water/ethanol mixtures.[23] This value lies substantially above the numbers obtained for a similar concentration of GAG in water-ethanol mixtures (200 mM) which vary between 41 and 25 °C at 74 and 50 mol% ethanol, respectively.[24]

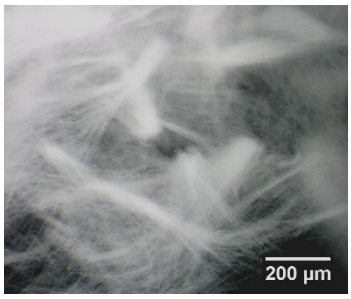

Figure 2. Microscopic image of a GHG hydrogel formed with 175 mM peptide concentration at pH=6.4.

Wide-angle X-ray scattering patterns were collected for precipitated GHG and for gels formed with 175 mM GHG at pH=6.47 (Figure S6). The diffraction rings are better resolved for the precipitated peptide. We integrated the 2D-patterns over an angle of 2π and observed the scattering spectra in q-space, shown in Figure S7 (cf. Material and Methods). The common peak of the spectra at 1.58 $Å^{-1}$ was normalized to 1. The peaks in the spectra appear at the same positions, though the spectrum of the gel exhibits lesser peak intensities. This observation suggests that the fibrils in the gel phase exhibit a crystalline structure similar to that in the precipitated peptide while the gel contains a more amorphous component. Peaks in 0.5-0.7$Å^{-1}$, 1-1.1$Å^{-1}$ and 1.4-1.6$Å^{-1}$ regions are tentatively assigned to inter-residue, inter-strand and inter-sheet of distances of a heterogeneous ensemble of β-sheets.[25] We are currently carrying out a thorough analysis of the WAXS data of GHG and the gel phases formed by other GxG peptides. The results will be reported in a future publication.

Next, we used vibrational spectroscopy to characterize the gel phase further. Note that these measurements had to be performed in D_2O to eliminate the overlap with the HOH water bending band and vibrational mixing between peptide modes (amide I) and water.[26,27] Hence, we had to use DCl and NaOD for adjusting the initial and final pD values. IR and VCD spectra of a 175 mM pH=6.39 sample measured over 20 h after incubation are shown in Figure 4. The cell was rotated approximately 120° between three measurements (the arbitrary position R1 as starting point, followed R2, and R3) of the same sample (cf. the inset of Figure 4). The VCD and IR of spectrum R2 were scaled so the IR peak intensity at 1595 cm^{-1} is identical to that of the R3 spectrum. This was done to allow for a comparison of the relative intensities of the respective VCD signals. The unscaled spectra are shown in Figure S8.

In order to properly interpret the spectra in Figures 4 and S9, we revisit the amide I' profiles in the earlier reported Raman, IR and VCD spectra of double and single protonated monomeric GHG.[13] (Figure S7). The doublet with peaks at 1656 and 1680 cm^{-1} is assignable to the amide I' modes of the tripeptide. In principle, one would attribute the former to the CO stretching

mode of the C-terminal peptide and the latter to the corresponding mode of the N-terminal peptide group, but excitonic coupling between the excited vibrational states mixes the wavefunctions of these states.[13] In both protonation states, the VCD signal of amide I is a weak negative couplet with an amplitude of ca. 0.02 $M^{-1}cm^{-1}$. It is diagnostic of a polyproline II/β-strand mixture of the central histidine residue.[13]

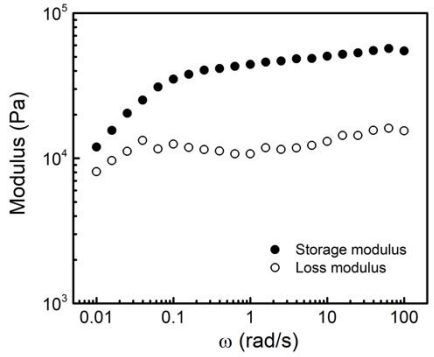

Figure 3. Rheological frequency sweep of storage modulus (G') and loss modulus (G") of a GHG hydrogel formed with 175 mM peptide concentration at pH=6.4.

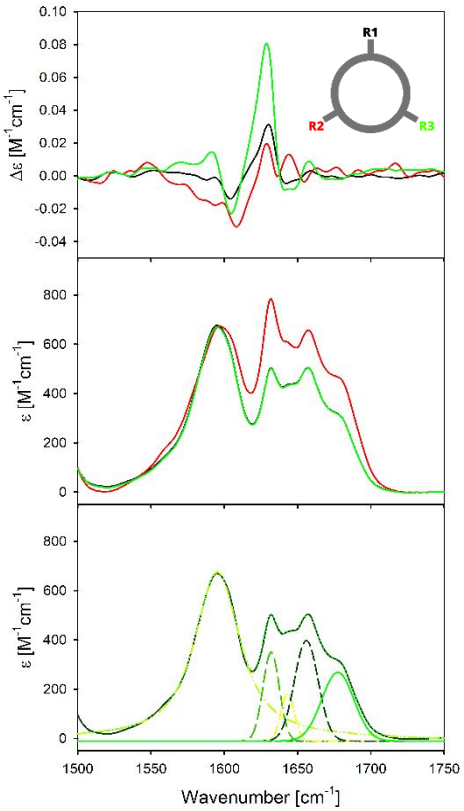

Figure 4. VCD (top), FT-IR (middle) and spectral decomposition of FTIR (bottom) spectra of 175 mM GHG at pD=6.39 in the region between 1500 and 1750 cm^{-1}. Sample was rotated approximately 120° between scans. The spectra are labelled as R1 (black), R2 (red), and R3 (green) in the text. Insert at top shows diagram of sample cell with the top of the cell for each rotation labelled. The spectral decomposition was performed with the R3 spectrum.

Apparently, the amide I' profiles depicted in Figure 4 are quite distinct from those in Figure S7. The amide I' profile of the gel phase has become more inhomogeneous. We subjected it to a spectral decomposition into sub-bands. The result is shown in the bottom panel of Figure 4. The band at 1595 cm^{-1} is Voigtian, while the ones from 1630– 1677 cm^{-1} are Gaussian. The spectral decomposition in Figure 4 is heuristic in nature because the observed band profile is in reality underlied by a multiplet of lines assignable to transitions into delocalized vibrational states.[30] The bands at 1656 and 1677 cm^{-1} are close to the band position obtained for monomeric protonated GHG in D_2O (1656 and 1680 cm^{-1}).[31] The two bands at 1632 and 1643 cm^{-1} are in the wavenumber range of amide I' bands assignable to β-sheet structures.[32,33] The wavenumber position depends on the number of incorporated strands (larger sheets shift the band to lower wavenumbers) and the geometry of the sheet (twisting reduces interstrand vibrational coupling and increase the amide I' peak wavenumber).[34–36] Our spectral analysis yielded a total fractional intensity of 0.26 for the two β-sheet bands. The real β-sheet content is likely higher because this conformation gives rise to a spectral continuum of excitonic transitions that covers the entire region between 1630 and 1690 cm^{-1}.[34,36] This continuum contributes to the 1656 and 1677 cm^{-1} band intensities obtained from our analysis.

The fibrilization on the scale shown in Figure 2 can be expected to produce an anisotropy of the sample which could produce linear as well as circular birefringence.[37,38] Therefore, after the first measurement (R1 in Figure 4) we rotated the sample twice by 120° and measured the IR and VCD spectra after each rotation (R2 and R3 in Figure 4). The IR spectrum observed after the first rotation exhibits an increased β-sheet signal at 1632 cm^{-1}. In terms of rotational strength and character the amide I' couplets in R1 and R2 are comparable with the negative couplet of the peptide monomer (Figure S9), but the positions of the negative and positive maxima now lie at the COO^- antisymmetric stretching band and the 1632 cm^{-1} sub-band of the amide I' profile, respectively. The corresponding VCD signal is on the same order of magnitude as that observed for the amide I' region of monomeric GHG.[31] The second rotation returned the IR spectrum to the same relative magnitudes. The VCD signal increased significantly. These observations suggest that the orientation of fibrils in the sample is somewhat anisotropic which causes some birefringence. The rather high wavenumber positions and the negligible rotational strength of the 1643 cm^{-1} band are indicative of untwisted β-sheet type oligomers.[34] The VCD associated with the 1595 and 1632 cm^{-1} band is clearly pronounced but less intense than observed for GAG fibrils.[10–12] Generally, ideal β-sheets are nearly planar and give rise to very weak VCD signals.[36] A strong VCD signal like the one associated with the 1632 cm^{-1} band suggests long helically twisted β-sheet tapes integrated in peptide fibrils. Such supramolecular structures generally give rise to either a negative or positive couplet in the region of highest amide I intensity.[11,12,39,40] Here, the negative maximum is shifted to the COO^- asymmetric stretching band region. The only plausible explanation for this observation is excitonic coupling between COO^- as and amide I' vibrations in adjacent strands where the C-terminal substitutes for the C=O group in interstrand excitonic coupling. The comparatively large wavenumber difference between these two bands reduces the mixing of wavefunctions in excitonic states compared with the interstrand coupling between amide I' modes with identical or similar intrinsic wavenumber positions. This explains why the observed couplet is less intense than that of GAG fibrils. Furthermore, we have to take into account that β-sheets

account only for 26% of the peptides. Hence, the real VCD signal would increase by a factor of 4 if all peptides were incorporated in fibrils.

Taken together our results suggest that deprotonated GHG forms a strong hydrogel in water. The sample spanning network is formed by large crystalline fibrils composed of β-sheet tapes. The pH at which fibrilization occurs varies with peptide concentration. Below 40 mM, no visible aggregation occurs irrespective of pH. In the region close to the boundary separating the gel phase from a less viscous phase of partially aggregated peptides (Figure 1), amorphous aggregates and β-sheet based helical twisted fibrils coexist. The degree of fibril crosslinking is sufficient to form a rather strong gel. Future investigations will focus on the peptide concentration and pH dependence of the gel phase characteristics.

Conflicts of interest

Research reported in this paper was supported by a grant from the National Science Foundation to R.S.S. and N.J.A. (DMR-170770) and an REU-supplement for the support of M.H. (DMR-1915781). M.H. was further supported by a grant from the Steinbright Career Development Center of Drexel University.

Notes and references

1 E. Gazit, *Prion*, 2007, **1**, 32–35.
2 L. Adler-Abramovich and E. Gazit, *Chem. Soc. Rev.*, 2014, **43**, 6881–6893.
3 R. V Ulijn, N. Bibi, V. Jayawarna, P. D. Thornton, S. J. Todd, R. J. Mart, A. M. Smith and J. E. Gough, *Mater. Today*, 2007, **10**, 40–48.
4 P. W. J. M. Frederix, G. G. Scott, Y. M. Abul-Haija, D. Kalafatovic, C. G. Pappas, N. Javid, N. T. Hunt, R. V. Ulijn and T. Tuttle, *Nat. Chem.*, 2015, **7**, 30–37.
5 I. W. Hamley, *Angew Chem Int Ed Engl*, 2007, **46**, 8128–8147.
6 E. R. Draper and D. J. Adams, *Chem. Soc. Rev.*, 2018, **47**, 3395–3405.
7 P. W. J. M. Frederix, R. V. Ulijn, N. T. Hunt and T. Tuttle, *J. Phys. Chem. Lett.*, 2011, **2**, 2380–2384.
8 A. Mahler, M. Reches, M. Rechtier, S. Cohen and E. Gazit, *Adv. Matec.*, 2006, **18**, 1365–1370.
9 G. Cheng, V. Castelletto, C. M. Moulton, G. E. Newby and I. W. Hamley, *Langmuir*, 2010, **26**, 4990–4998.
10 B. Milorey, S. Farrell, S. E. Toal and R. Schweitzer-Stenner, *Chem. Commun.*, , DOI:10.1039/c5cc06097d.
11 S. Farrell, D. DiGuiseppi, N. Alvarez and R. Schweitzer-Stenner, *Soft Matter*, 2016, **12**, 6096–6110.
12 D. DiGuiseppi, L. Thursch, N. J. Alvarez and R. Schweitzer-Stenner, *Soft Matter*, 2019, **15**, 3418–3431.
13 D. DiGuiseppi and R. Schweitzer-Stenner, *J. Raman Spectrosc.*, , DOI:10.1002/jrs.4885.
14 V. Jayawarna, M. Ali, T. A. Jowitt, A. F. Miller, A. Saiani, J. E. Gough and R. V. Ulijn, *Adv. Mat.*, 2006, **18**, 611–614.
15 R. Otter, C. M. Berac, S. Seiffert and P. Besenius, *Eur. Polym. J.*, 2019, **110**, 90–96.
16 K. J. C. Van Bommel, C. Van Der Pol, I. Muizebelt, A. Friggeri, A. Heeres, A. Meetsma, B. L. Feringa and J. Van Esch, *Angew. Chemie - Int. Ed.*, 2004, **43**, 1663–1667.
17 T. J. Moyer, J. A. Finbloom, F. Chen, D. J. Toft, V. L. Cryns and S. I. Stupp, *J. Am. Chem. Soc.*, 2014, **136**, 14746–14752.
18 B. F. Lin, K. A. Megley, N. Viswanathan, D. V. Krogstad, L. B. Drews, M. J. Kade, Y. Qian and M. V. Tirrell, *J. Mater. Chem.*, 2012, **22**, 19447–19454.
19 V. Castelletto, G. Cheng, B. W. Greenland, I. W. Hamley and P. J. F. Harris, *Langmuir*, 2011, **27**, 2980–2988.
20 R. L. Thurlkill, G. R. Grimsley, J. M. Scholtz and C. N. Pace, *Protein Sci.*, 2006, **15**, 1214–1218.
21 A. Chakrabartty, T. Kortemme, S. Padmanabhan and R. . Baldwin, *Biochemistry*, 1993, **32**, 5560–5565.
22 S. Bhattacharjee, G. Tóth, S. Lovas and J. D. Hirst, *J. Phys. Chem. B*, 2003, **107**, 8682–8688.
23 L. Thursch, D. DiGuiseppi, T. Lewis, R. Schweitzer-Stenner and N. J. Alvarez, *J. Colloid Interface Sci.*, 2020, **564**, 499–509.
24 L. Thursch, D. DiGuiseppi, N. Alvarez and R. Schweitzer-Stenner, *J. Coll. Int. Sci.*
25 L. Kreplak, J. Doucet, P. Dumas and F. Briki, *Biophys. J.*, 2004, **87**, 640–647.
26 G. Sieler and R. Schweitzer-Stenner, *J. Am. Chem. Soc.*, 1997, **119**, 1720–1726.
27 N. V. Ilawe, A. E. Raeber, R. Schweitzer-Stenner, S. E. Toal and B. M. Wong, *Phys. Chem. Chem. Phys.*, , DOI:10.1039/c5cp03646a.
28 R. Schweitzer-Stenner, A. Hagarman, S. Toal, D. Mathieu and H. Schwalbe, *Proteins Struct. Funct. Bioinforma.*, , DOI:10.1002/prot.24225.
29 A. Hagarman, T. J. Measey, D. Mathieu, H. Schwalbe and R. Schweitzer-Stenner, *J. Am. Chem. Soc.*, , DOI:10.1021/ja9058052.
30 A. Kumar, R. Schweitzer-Stenner and B. M. Wong, *Chem. Comm.*, 2019, **55**, 5701–5704.
31 D. DiGuiseppi and R. Schweitzer-Stenner, *J. Raman Spectrosc.*, 2016, **47**, 1063–1072.
32 S. Krimm and J. Bandekar, *Adv Protein Chem*, 1986, **38**, 181–364.
33 A. Barth, *Prog Biophys Mol Biol*, 2000, **74**, 141–173.
34 R. Schweitzer-Stenner, *J. Phys. Chem. B*, 2012, **116**, 4141–4153.
35 C. Lee and M. Cho, *J. Phys. Chem. B*, 2004, **108**, 20397–20407.
36 P. Bour and T. A. Keiderling, *J. Mol. Struct.*, 2004, **675**, 95–105.
37 T. Buffeteau, F. Lagugné-Labarthet and C. Sourisseau, *Appl. Spectrosc.*, 2005, **59**, 732–745.
38 M. Wolffs, S. J. George, Ž. Tomović, S. C. J. Meskers, A. P. H. J. Schenning and E. W. Meijer, *Angew. Chemie - Int. Ed.*, 2007, **46**, 8203–8205.
39 T. J. Measey and R. Schweitzer-Stenner, *J. Am. Chem. Soc.*, 2011, **133**, 1066–1076.
40 S. Ma, X. Cao, M. Mak, A. Sadik, C. Walkner, T. B. Freedman, I. K. Lednev, R. K. Dukor and L. A. Nafie, *J. Am. Chem. Soc.*, 2007, **129**, 12364–12365.

